# An Innovative Multiresolution Approach for DOA Estimation Based on a Support Vector Classification

Massimo Donelli, *Member, IEEE*, Federico Viani, Paolo Rocca, and Andrea Massa, *Member, IEEE*

***Abstract*—The knowledge of the directions of arrival (DOAs) of the signals impinging on an antenna receiver enables the use of adaptive control algorithm suitable for limiting the effects of interferences and increasing the gain towards the desired signals in order to improve the performances of wireless communication systems. In this paper, an innovative multi-resolution approach for the real-time DOA estimation of multiple signals impinging on a planar array is presented. The method is based on a support vector classifier and it exploits a multi-scaling procedure to enhance the angular resolution of the detection process in the regions of incidence of the incoming waves. The data acquired from the array sensors are iteratively processed with a support vector machine (SVM) customized to the problem at hand. The final result is the definition of a map of the probability that a signal impinges on the antenna from a fixed angular direction. Selected numerical results, concerned with both single and multiple signals, are provided to assess potentialities and current limitations of the proposed approach.**

***Index Terms*—Classification, direction of arrival (DOA) estimation, multiresolution, planar arrays, support vector machine.**

## I. Introduction

In THE LAST decades, the technology of adaptive antenna arrays has been greatly advanced and applied to many mobile and wireless communication systems [1], [2]. Within this framework, the antenna beam-forming plays an important role and the estimation of the directions of arrival (DOAs) of signals impinging on the array is a crucial task in order to enhance the spatial diversity and consequently the spectral efficiency. As a matter of fact, such an information enables the generation or steering of the radiation pattern with a maximum towards the desired signals and nulls along the directions of interfering signals [3], [4]. The effects of interferences are mitigated and both the gain and the performance of the whole communication system are enhanced. For such reasons, the estimation of the DOAs of unknown interfering and desired signals is of great interest and it is still an open problem as confirmed by the number of papers published on this topic.

In the scientific literature, several methods have been proposed for the direction finding of multiple signals impinging on an array of narrow band sensors. Among them, the most widely known and used are estimation of signal parameters via rotational invariance technique (ESPRIT) [5]–[7] and multiple signal classification (MUSIC) [8], [9]. Other approaches based on the maximum likelihood (ML) DOA estimation have been proposed [10], [11], as well.

In the last years, great attention has been also paid to the use of learning-by-examples (LBE) techniques. LBE-based approaches are able to provide a good trade-off between accuracy and convergence, which is mandatory for real time systems where fast reactions are required. Furthermore, they satisfactory deal with unknown configurations (i.e., different from those "learned" during the training process) thanks to their generalization capability. Within this framework, the benefits of using radial basis function neural networks (RBFNN) have been carefully analyzed in [12]. As a matter of fact, neural networks (NNS) are suitable in approximating nonlinear functions as those in DOAs estimation. Moreover, they can be easily implemented in analog circuits. An improved RBFNN-based approach has been presented by the same authors of [12] in [13] to address the problem of tracking an unknown number of multiple sources when no *a-priori* information on the number of impinging signals is available. More specifically, the region above the antenna has been partitioned into angular sectors and each sector "assigned" to a simpler NN, thus reducing with respect to [12] the problem complexity as well as the computational burden of the learning phase. Towards this end, each network has been trained to detect the subset of incoming signals that impinge on the corresponding angular sector. Accordingly, only those NNs of the regions where the signals have been detected in the first stage of the process are activated in the second one to estimate the DOAs of the incoming signals.

More recently, some techniques based on support vector machines (SVMs) [14] have been analyzed to profitably exploit their solid mathematical foundation in statistical learning theory [15]. The main advantages of those approaches lie in their ability to deal with various and complex electromagnetic problems [16], [17], and, analogously to NNs, in an easy hardware implementation [18]. As far as the DOA estimation is concerned, a support vector regression (SVR) procedure has been presented in [19] when dealing with linear arrays. In such a case, a SVM has been used to estimate the DOA of each impinging electromagnetic wave starting from a set of known input-output examples where the DOAs of the signals were uniformly distributed in the whole angular region above the receiver. Despite the generalization capability of the SVR-based method, an *a-priori* information on the number of sources and pre-fixed angular separations between the DOAs (as in [12])

Manuscript received August 06, 2008; revised January 20, 2009. First published June 05, 2009; current version published August 05, 2009.

The authors are with the Department of Information and Communication Technology, University of Trento, 38050 Trento, Italy (e-mail: andrea.massa@ing.unitn.it; massimo.donelli@dit.unitn.it; federico.viani@dit.unitn.it; paolo.rocca@dit.unitn.it).

Color versions of one or more of the figures in this paper are available online at http://ieeexplore.ieee.org.

Digital Object Identifier 10.1109/TAP.2009.2024485

have been considered to increase the reliability of the estimation procedure. An extension of such a model has been presented in [20] and experimentally validated in [21] successively.

In this paper, an innovative procedure for real-time direction finding of signals impinging on a planar array of electromagnetic sensors is presented. The problem of the DOAs estimation is formulated as a two step procedure, where the first step is aimed at determining the decision function that correctly classifies whatever input pattern by means of a SVM-based approach. In the second step, the output of the decision function is mapped into the *a-posteriori* probability that a signal impinges on the antenna from a fixed direction. In order to increase the accuracy of the estimation process and to reduce the computational burden affecting other DOAs procedures, the proposed two-step strategy is nested into an iterative multi-scaling process [22]. Accordingly, the resolution accuracy is improved only in those angular regions where the unknown sources are supposed to be located at the previous iteration. More specifically, the algorithm first determines a coarse probability map of the DOAs starting from a training set where the incoming signals are nonuniformly distributed along the elevation direction, $\theta$, and the azimuthal one, $\phi$. Then, the SVM is used to classify the input test dataset at successive resolution levels by performing a kind of synthetic zoom in the angular regions of interest (ARoIs) where a higher probability is detected and considering the same training set, thus performed only once and off-line. Concerning the antenna architecture and unlike [13] and [20], planar arrays of sensors are considered since linear arrays lack the ability to scan in 3D-space and the estimation of both the elevation $\theta$ and the azimuth $\phi$ angles is crucial and has many applications in various fields of engineering. For instance, a complete DOA information it is possible to improve the coverage of transmission in wireless communications by avoiding interferences and enhancing the system capacity [23]. More specifically, planar arrangements are very attractive in mobile communications with portable devices where the main beam must be scanned in any direction [24]. Moreover, the number of impinging signals is unknown as well as their directions belonging to the whole angular range above the planar antenna system (i.e., $\theta \in [0 : 90^{\circ}]$ and $\phi \in [0 : 360^{\circ}]$).

The paper is organized as follows. The formulation of the iterative two-step multi-resolution DOA approach (in the following denoted by the acronym IMSA-SVM) is described in Section II. In order to show the innovative features of the approach and to assess its effectiveness, a selected set of numerical results concerned with both single and multiple signals is reported and discussed (Section III). Moreover, some comparisons with state-of-the-art techniques are also reported. Finally, some conclusions are drawn in Section IV.

## II. Mathematical Formulation

Let us consider a planar array of $M$ isotropic elements displaced on a regular and rectangular grid with inter-element spacing $d$ on the $x-y$ plane. A set of $I$ electromagnetic waves impinge on the array from unknown angular directions $(\theta_i,\ \phi_i),\ i = 1,\ldots,I$, as sketched in Fig. 1. The signals, supposed to be narrow-band and centered at the carrier frequency $f$ ($\lambda$ being the corresponding free-space wavelength),

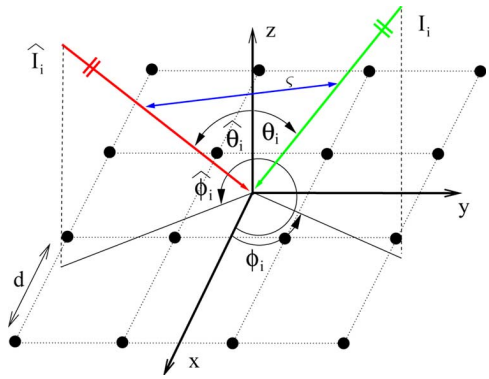


Fig. 1. Planar array geometry.

are generated by a set of electromagnetic sources placed in the far-field of the receiving antenna. The open-circuit voltage at the output of the $m$th sensor can be expressed as [20]

$$v_m = \sum_{i=1}^{I} \left\{ a_m\left(\theta_i,\phi_i\right) \left[ \underline{E}_i\left(x_m,\ y_m\right) \cdot \underline{e}_m \right] \right\} + g_m, \qquad m = 1,\ldots,M \quad (1)$$

where $a_m\left(\theta_i,\phi_i\right) = e^{j2\pi/\lambda sin\theta_i(x_m cos\phi_i + y_m sin\phi_i)}$, $(x_m,\ y_m)$ being the location of the $m$th sensor expressed in wavelength, and $g_m$ is the background random noise at the $m$th locations. The noise samples are supposed to be statistically independent and characterized by a random Gaussian distribution with zero mean value. Moreover, $\underline{E}_i$ and $\underline{e}_m$ are the electric field associated to the $i$th impinging wave and the effective length of the $m$th array element.

According to the guidelines described in [3] and [4] about the control of adaptive/smart antennas, the solution of the DOAs estimation problem is based also in this work on the measurement of the total correlation matrix, defined as

$$\underline{\underline{\Phi}} = E\left\{ \underline{v} \cdot \underline{v}^{*} \right\} \quad (2)$$

where $\underline{v} = \{v_m;\ m = 1,\ldots,M\}$ and the superscript $^*$ stands for complex conjugation, at the output of the planar array since it contains sufficient information on the received signals [13]. From a statistical point of view, the problem at hand can be formulated as the definition of the probability map of the angular incidence of the incoming waves starting from the knowledge of the total correlation matrix $\underline{\underline{\Phi}}$. Towards this end, let us partition the angular region above the array into a two-dimensional lattice of $H = H_\theta \times H_\phi$ cells, each one corresponding to an angular sector of sides $\Delta\theta$ and $\Delta\phi$ [Fig. 2(a)]. The status $\chi_h$ of each cell can be *empty* $[\chi_h = \chi\left(\theta_h,\phi_h\right) = -1]$, if any signal impinges on the array from the angular region identified by the same cell, or *occupied* $[\chi_h = \chi\left(\theta_h,\phi_h\right) = 1]$, otherwise. Accordingly, the original problem can be stated as follows: "*find the a-posteriori probability function* $Q\left(\theta,\phi\right)$ *given a measured value of the total correlation matrix* $\underline{\underline{\Phi}}$ *at the receiver*." Mathematically, $Q\left(\theta,\phi\right)$ can be also expressed as the linear combination of the nonoverlapping basis functions $B_h\left(\theta,\phi\right), h = 1,\ldots,H$ defined over

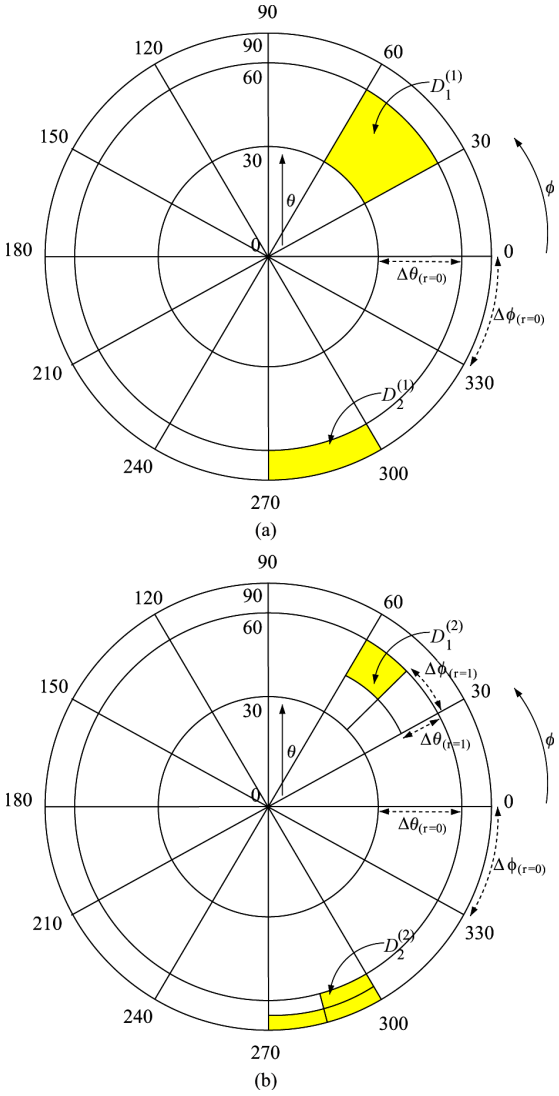


Fig. 2. IMSA-DOA Procedure—Angular region partitioning and ARoIs identification at the steps $s = 1$ (a) and $s = 2$ (b).

the angular lattice

$$Q(\theta,\phi) = \sum_{h=1}^{H} q(\theta_h,\phi_h)\, B_h(\theta,\phi) \tag{3}$$

where the weighting coefficient $q(\theta_h,\phi_h)$ is the probability value that a wave impinges on the array from the $h$th angular sector [i.e., $q(\theta_h,\phi_h) = Pr\{\chi_h = 1; |\underline{\underline{\Phi}}\}$] and $B_h(\theta,\phi) = 1$ if $(\theta,\phi)$ belongs to the $h$th cell and $B_h(\theta,\phi) = 0$ otherwise.

In order to improve the achievable angular resolution, a multiresolution representation of the unknown function $Q(\theta,\phi)$ is looked for [Fig. 2(b)—$r = 1$] by exploiting an iterative process analogously to [22]. More specifically, the probability function is expressed at the $s$th step of the iterative procedure as a twofold summation of shifted and dilated spatial basis functions

$$Q^{(s)}(\theta,\phi) = \sum_{r=0}^{R(s)} \sum_{h(r)=1}^{H(r)} q^{(s)}\left(\theta_{h(r)},\phi_{h(r)}\right) B_{h(r)}(\theta,\phi) \qquad s = 1,\ldots,S_{\text{opt}} \tag{4}$$

$r$ being the resolution index and $R(s) = s - 1$. The summation over $r$ ranges from 0 [Fig. 2(a)], which corresponds to the largest characteristic length scale, to $R(s)$ [Fig. 2(b)], which corresponds to the smallest angular basis-function support at the $s$th scaling step. For a given value of $r$, $H(r) = H_\theta^{(r)} \times H_\phi^{(r)}$ is the number of nonoverlapped basis functions centered in the angular sub-domain represented at the $r$th resolution. Accordingly, the iterative DOA detection procedure is aimed at locating the terms of small length scale at those ARoIs [e.g., the shaded cells in Fig. 2(a)–(b)] where the signals are supposed to impinge with higher probability.

In order to profitably exploit the multiresolution representation of the *a-posteriori* probability function (4) and solving the arising DOA problem, the following multistep classification process is performed by means of a SVM-based technique. More in detail

- **Step 0**— *SVM Training Phase*. The SVM is trained once and off-line starting from the knowledge of a set of known examples (i.e., input/output relationships)

$$\left\{\left[\underline{\underline{\Phi}},\ (\theta_n,\phi_n),\ \chi_n = \chi(\theta_n,\phi_n);\ n = 1,\ldots,N\right]^{(t)} \quad t = 1,\ \ldots,T\right\} \tag{5}$$

called *training set*, where $T$ is the number of training data. The $N$ samples of each training data are composed by $I(t)$ examples concerned with angular positions $(\theta_i,\phi_i)$, $i = 1,\ldots,I(t)$, $I(t) \le I_{\max}$ where a signal impinges on the array [i.e., *occupied* directions—$\chi(\theta_i,\phi_i) = 1;\ i = 1,\ldots,I(t)$], while the remaining $F(t) = N - I(t)$ are related to *empty* directions [i.e., $\chi(\theta_f,\phi_f) = -1;\ f = 1,\ldots,F(t)$].
Starting from the knowledge of the *training set*, the problem turns out to be the definition of a suitable discriminant function $\hat{\Im}$

$$\hat{\Im} : \underline{\underline{\Phi}} \rightarrow [\chi(\theta_h,\phi_h);\ h = 1,\ldots,H] \tag{6}$$

that separates the two classes $\chi(\theta,\phi) = 1$ and $\chi(\theta,\phi) = -1$ on the basis of the total correlation matrix $\underline{\underline{\Phi}}$ measured at the output of the planar array. In order to approach the problem with a single classifier, the problem at hand is reformulated as that of building the following single output function

$$\hat{\Im} : \left[\underline{\underline{\Phi}},\ (\theta_n,\phi_n);\ n = 1,\ \ldots,N\right] \rightarrow \chi(\theta_h,\phi_h) \qquad h = 1,\ldots,H. \tag{7}$$

Towards this purpose and according to the SVM theory [15], the following linear decision function is adopted

$$\hat{\Im}\left\{\underline{\varphi}\left(\underline{\underline{\Phi}},\ (\theta_n,\phi_n)\right)\right\} = \underline{w}\cdot\underline{\varphi}\left(\underline{\underline{\Phi}},\ (\theta_n,\phi_n)\right) + b \qquad n = 1,\ldots,N. \tag{8}$$

$\hat{\Im}$ is determined in a space (called "*feature space*") with a higher dimensionality than the original input data space

and obtained through the nonlinear operator $\underline{\varphi}(\cdot)$ [15]. The unknown terms $\underline{w}$ and $b$, which unequivocally define the decision hyperplane $\hat{\Im}$, are the normal vector and a bias, respectively. They are computed during the *Training Phase* according to the guidelines described in [17];

- **Step 1**—*Low-Order DOA Estimation* $(s = 1)$. At the first step, a coarse probability map [(4)—$s = 1$] is determined by means of the SVM classifier mapping the decision function $\hat{\Im}$ into the *a-posteriori* probability function.
  The unknown probability coefficients $q^{(s)}(\theta_h, \phi_h)\big]_{s=1}$, $h = 1, \ldots, H$ are approximated with a sigmoid function [15] as follows

$$q^{(s)}(\theta_h, \phi_h) = \frac{1}{1+\exp[\gamma \hat{\Im}\{\underline{\varphi}(\underline{\underline{\Phi}}, (\theta_h, \phi_h))\} + \nu]} \tag{9}$$

  where $\gamma$ and $\nu$ are two parameters computed according to a fitting process [17] starting from a subset of the $T$ training data of the *Training Set*;
- **Step 2**—*IMSA-SVM Process* $(s \geq 1)$.
  — **Step 2.a**—*Angular Regions of Interest* $(ARoIs)$ *Identification* $(s \leftarrow s+1)$. Starting from the probability map previously (i.e., at the $s-1$th iteration) determined, such a step is aimed at identifying the angular sectors $D_\ell^{(s)}$, $\ell = 1, \ldots, L(s)$ where the signals are supposed to impinge in order to improve the resolution only in those regions and enhance the accuracy of the DOA estimation. Towards this end, first the values of the function $Q^{(s-1)}(\theta, \phi)$ are scaled, thus defining the following new set of normalized probability coefficients

$$p^{(s-1)}\left(\theta_{h(r)}, \phi_{h(r)}\right) = \frac{q^{(s-1)}\left(\theta_{h(r)}, \phi_{h(r)}\right)}{q_M - q_m} + \frac{q_m}{q_m - q_M} P \quad h(r) = 1, \ldots, H(r)\ r = 0, \ldots, R(s). \tag{10}$$

  where $q_M = \max_{r=0,\ldots,R(s)} \left\{\max_{h(r)=1,\ldots,H(r)} \left[q^{(s-1)}\left(\theta_{h(r)}, \phi_{h(r)}\right)\right]\right\}$ and $q_m = \min_{r=0,\ldots,R(s)} \left\{\min_{h(r)=1,\ldots,H(r)} \left[q^{(s-1)}\left(\theta_{h(r)}, \phi_{h(r)}\right)\right]\right\}$.
  Successively, the new probability function

$$P^{(s-1)}(\theta, \phi) = \sum_{r=0}^{R(s-1)} \sum_{h(r)=1}^{H(r)} p^{(s-1)}\left(\theta_{h(r)}, \phi_{h(r)}\right) B_{h(r)}(\theta, \phi)$$

  is thresholded by nulling the scaled coefficients greater than a user-defined threshold $\eta$. Finally, the thresholded function

$$P_{th}^{(s-1)}(\theta, \phi) = \sum_{r=0}^{R(s-1)} \sum_{h(r)=1}^{H(r)} p_{th}\left(\theta_{h(r)}, \phi_{h(r)}\right) B_{h(r)}(\theta, \phi) \tag{11}$$

  where $p_{th}\left(\theta_{h(r)}, \phi_{h(r)}\right) = p^{(s-1)}\left(\theta_{h(r)}, \phi_{h(r)}\right)$ if $p^{(s-1)}\left(\theta_{h(r)}, \phi_{h(r)}\right) > \eta$ and $p_{th}\left(\theta_{h(r)}, \phi_{h(r)}\right) = 0$ otherwise, allows one to identify the ARoIs, $D_\ell^{(s)}$, $\ell = 1, \ldots, L(s)$ defined as those angular sub-domains where $P_{th}^{(s-1)}(\theta, \phi) \neq 0$;
  — **Step 2.b**—*Multiresolution DOA Estimation*. A synthetic zoom is performed by refining the representation of the unknown function $Q^{(s)}(\theta, \phi)$ and increasing the angular resolution $(r \leftarrow r+1)$ only in the ARoIs identified at (*Step 2.a*). Therefore, the multiresolution *a-posteriori* probability function (4) is updated [1] by setting $Q^{(s)}(\theta, \phi) = P_{th}^{(s-1)}(\theta, \phi)$ and computing the new highest resolution coefficients, $q^{(s)}\left(\theta_{h(r)}, \phi_{h(r)}\right)$, when $(\theta, \phi) \in D_\ell^{(s)}$, $\ell = 1, \ldots, L(s)$ as in (9);
- **Step 3**—*Termination Criterion* $(s = S_{\text{opt}})$. The sequence of operations of *Step 2* is repeated until both the dimensions and the number of ARoIs between two consecutive cycles are stationary [i.e., $L(s) = L(s-1)$ and the variations of the dimensions of the ARoIs are not greater than the highest angular resolution at the $s$th step, $\Delta_{\min}^{(s)} = min\left\{\Delta\theta_{R(s)}^{(s)}, \Delta\phi_{R(s)}^{(s)}\right\}$].

## III. Numerical Simulations and Results

In order to assess the effectiveness and reliability of the proposed approach, an exhaustive set of numerical experiments has been performed and some selected results will be reported in the following for illustrative purposes. The remaining of this section will firstly (Section III-A) illustrate the behavior of the multi-scaling procedure also in comparison with other state-of-the-art approaches for DOA estimation. The second part (Section III-B) will be devoted to analyze the potentialities and current limitations of the IMSA-SVM approach when dealing with various and challenging electromagnetic scenarios. In such a framework, some configurations in which conventional state-of-the-art signal subspace-based array processing techniques cannot be applied are also dealt with in order to point out the enhanced range of applicability of SVM approaches. Finally, a uniform array of $\lambda/2$-dipoles is considered (Section III-C) to verify the suitability and reliability of the proposed method in correspondence with a realistic array modelling With reference to the geometry shown in Fig. 1, a square planar array of $M = 16$ isotropic radiators spaced by $d = \lambda/2$ is considered. The power of the impinging signals has been set to $P_i = 30$ dB, $i = 1, \ldots, I$ above the level of the background noise.

Concerning the training set, the following setup $T = 400$ and $I_{\max} = 4$ has been assumed and the SVM classifier has been trained once and off-line on the same data set whatever the test experiment. As regards to the $T = \sum_{i=1}^{I_{\max}} T_i$ training examples, different scenarios have been considered, $T_i = 100$ being the number of configurations with $i$ signals. Moreover, the actual DOAs of the signals of the training data have been randomly

[1]It is worth noting that at the $s$th step of the multi-scaling procedure only the angular ranges belonging to the ARoIs are processed by the SVM classifier with a non-negligible saving of computational resources.

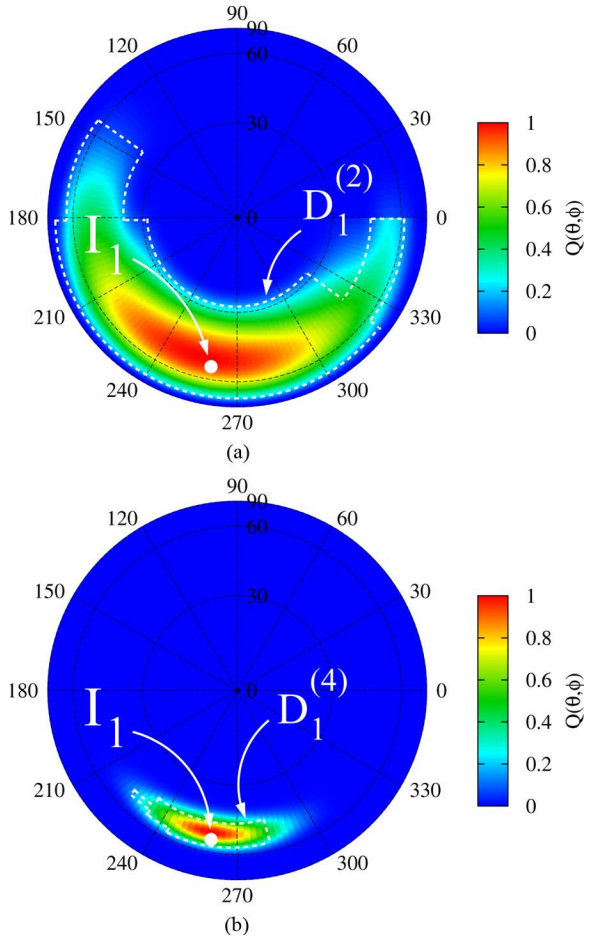


Fig. 3. *Single signal scenario*, $I = 1$—Probability map determined by the IMSA-DOA procedure at: (a) $s = 2$, (b) $s = S_{\text{opt}} = 4$.

chosen in a discrete grid of locations $(\theta_n, \phi_n)$, $n = 1, \ldots, N$ belonging to the the angular region above the antenna

$$\begin{cases} \theta_n = \theta_0 + \left\lfloor \frac{n-1}{\sqrt{N}} \right\rfloor \Delta\theta \\ \phi_n = \phi_0 + \left\lceil \frac{n-1}{\sqrt{N}} \right\rceil \Delta\phi \end{cases}, \quad n = 1, \ldots, N \tag{12}$$

$\lfloor \cdot \rfloor$ and $\lceil \cdot \rceil$ being the floor function and the ceiling function, respectively. Moreover, in order to fully assess the generalization properties of the SVM-based approach, the DOAs of the test examples are different from those of the training dataset.

### A. Single Signal Scenario—Comparative Assessment

The first experiment deals with the DOA detection of a single signal and a *test set* of $T_1^{(\text{test})} = 100$ examples related to the single-signal scenario has been considered. An illustrative description of the behavior of the proposed IMSA-SVM approach is shown in Fig. 3 dealing with the "representative" (of the method performance on the whole test dataset) configuration of a signal coming from $(\theta_1 = 53°,\ \phi_1 = 260°)$. At the first step $(s = 1)$, the planar angular region $D^{(1)}$ is partitioned into $H^{(s)} = 81$ cells (being $\Delta\theta_{(r)}^{(s)} = 10°$ and $\Delta\phi_{(r)}^{(s)} = 40°$, $r = 0$, the angular steps along the elevation direction, $\theta$, and the azimuthal one, $\phi$, respectively) and a coarse DOA probability map is determined following the procedure described in Section II (*Step 1*). Then, the multi-scaling procedure takes place $(s \geq 2)$. The ARoIs are identified and partitioned into $H_{R(s)}^{(2)}\Big|_{R(s)=s-1} = 81$ cells with an angular resolution of $\Delta\theta_{(1)}^{(2)} = 5°$ and $\Delta\phi_{(1)}^{(2)} = 20°$. For the sake of space, only the DOA probability map obtained at the end of the second step $(s = 2)$ is shown in Fig. 3(a). The procedure is then iterated until $s = S_{\text{opt}} = 4$ $[R(S_{\text{opt}}) = 3]$ with the final result reported in Fig. 3(b) characterized by an angular resolution in $D_1^{(4)}$ equal to $\Delta\theta_{(3)}^{(4)} = 1.25°$ and $\Delta\phi_{(3)}^{(4)} = 5°$. As it can be observed (Fig. 3), the region with higher probability of incidence turns out to be closer and closer to the actual angular location of the signal when increasing the step number. Quantitatively such an event can be analytically quantified by computing the values of the *location index* $\varsigma^{(s)}$ (Fig. 1) and of the *incidence area* $\psi^{(s)}$ defined as follows

$$\varsigma^{(s)} = \frac{\Phi^{(s)}}{\max\left\{\Phi^{(s)}\right\}} \times 100 \tag{13}$$

where, see equation at the bottom of the page, and

$$\psi^{(s)} = \pi \left\{ \frac{\sum_{r=0}^{R(s)} \sum_{h(r)=1}^{H(r)} \left\{ \frac{\varsigma_{h(r)}^{(s)} q^{(s)}\left(\theta_{h(r)}, \phi_{h(r)}\right)}{\max_{h(r)}\left\{q^{(s)}\left(\theta_{h(r)}, \phi_{h(r)}\right)\right\}} \right\}}{\sum_{r=0}^{R(s)} \sum_{h(r)=1}^{H(r)} \left\{ \frac{q^{(s)}\left(\theta_{h(r)}, \phi_{h(r)}\right)}{\max_{h(r)}\left\{q^{(s)}\left(\theta_{h(r)}, \phi_{h(r)}\right)\right\}} \right\}} \right\}^2 \tag{14}$$

being $\varsigma_{h(r)}^{(s)} = \left[ \left( \sin\theta_{h(r)} \cos\phi_{h(r)} - \sin\hat{\theta}^{(s)} \cos\hat{\phi}^{(s)} \right)^2 + \left( \sin\theta_{h(r)} \sin\phi_{h(r)} - \sin\hat{\theta}^{(s)} \sin\hat{\phi}^{(s)} \right)^2 + \left( \cos\theta_{h(r)} - \cos\hat{\theta}^{(s)} \right)^2 \right]^{1/2}$, $(\theta,\ \phi)$ are the actual coordinates of the signal incidence point, whereas $\left(\hat{\theta},\ \hat{\phi}\right)$

$$\begin{aligned} \hat{\theta}^{(s)} &= \frac{\sum_{r=0}^{R(s)} \sum_{h(r)=1}^{H(r)} \left\{ \theta_{h(r)} q^{(s)}\left(\theta_{h(r)}, \phi_{h(r)}\right) \right\}}{\sum_{r=0}^{R(s)} \sum_{h(r)=1}^{H(r)} \left\{ q^{(s)}\left(\theta_{h(r)}, \phi_{h(r)}\right) \right\}} \\ \hat{\phi}^{(s)} &= \frac{\sum_{r=0}^{R(s)} \sum_{h(r)=1}^{H(r)} \left\{ \phi_{h(r)} q^{(s)}\left(\theta_{h(r)}, \phi_{h(r)}\right) \right\}}{\sum_{r=0}^{R(s)} \sum_{h(r)=1}^{H(r)} \left\{ q^{(s)}\left(\theta_{h(r)}, \phi_{h(r)}\right) \right\}} \end{aligned} \tag{15}$$

identify the center of the $\ell$th ARoI where the signal/signals is/are supposed to impinge. As a matter of fact, the value of the location index reduces from $\varsigma^{(1)} = 13.17$ down to $\varsigma^{(S_{\text{opt}})} =$

$$\Phi^{(s)} \triangleq \sqrt{\left(\sin\theta\cos\phi - \sin\hat{\theta}^{(s)}\cos\hat{\phi}^{(s)}\right)^2 + \left(\sin\theta\sin\phi - \sin\hat{\theta}^{(s)}\sin\hat{\phi}^{(s)}\right)^2 + \left(\cos\theta - \cos\hat{\theta}^{(s)}\right)^2}$$

TABLE I
STATISTICS OF THE AVERAGED PERFORMANCE INDEXES ($\hat{\varsigma} = \sum_{i=1}^{I} \varsigma^{(i)}$ AND $\hat{\psi} = \sum_{i=1}^{I} \psi^{(i)}$) FOR DIFFERENT SIGNAL CONFIGURATIONS ($I = 1, 2, 3, 4$)

| | *Min* | *Max* | *Avg* | *Var* |
|---|---|---|---|---|
| | *Single Signal* ($I = 1$) | | | |
| $\hat{\varsigma}$ | 0.16 | 43.25 | 2.81 | 8.76 |
| $\hat{\psi}$ | 0.02 | 9.14 | 0.25 | 1.35 |
| | *Multiple Signals* ($I = 2$) | | | |
| $\hat{\varsigma}$ | 0.31 | 58.47 | 4.51 | 8.56 |
| $\hat{\psi}$ | 0.007 | 11.05 | 0.28 | 1.54 |
| | *Multiple Signals* ($I = 3$) | | | |
| $\hat{\varsigma}$ | 0.38 | 17.35 | 5.55 | 2.14 |
| $\hat{\psi}$ | 0.009 | 0.37 | 0.15 | 0.34 |
| | *Multiple Signals* ($I = 4$) | | | |
| $\hat{\varsigma}$ | 0.47 | 70.72 | 17.29 | 13.58 |
| $\hat{\psi}$ | 0.005 | 1.89 | 0.17 | 0.69 |

2.53 (being $\varsigma^{(2)} = 4.10$ and $\varsigma^{(3)} = 2.87$). Analogously, $\psi^{(1)} = 2.74$, $\psi^{(2)} = 0.94$, $\psi^{(3)} = 0.36$, until $\psi^{(S_{\text{opt}})} = 0.14$. As regards to the whole set of test examples, the statistics of the "convergence" values of the indexes (13) and (14) are given in the first block of Table I.

In order to get an insight into the advantages of the proposed multi-resolution approach over the classification single-step techniques, a bare DOA SVM-based method has been considered and applied to the same test example. To fairly compare the two methods, the same training dataset has been used. Moreover, the same angular resolution has been adopted in both cases. Towards this purpose, an angular lattice characterized by a uniform grid whose cell side was equal to the finest discretization of the multi-resolution procedure (i.e., $\Delta\theta = \Delta\theta_{(3)}^{(4)}$ and $\Delta\phi = \Delta\phi_{(3)}^{(4)}$), has been defined over the whole angular investigation domain of the single step SVM approach. As it can be observed [Fig. 4(a)], although the value of $\varsigma$ is quite close to that of the IMSA strategy (i.e., $\varsigma\rfloor_{\text{IMSA-SVM}} = 2.53$ versus $\varsigma\rfloor_{\text{SVM}} = 3.14$), the extension of the incidence area turns out to be significantly wider ($\psi\rfloor_{\text{IMSA-SVM}} = 0.14$ versus $\psi\rfloor_{\text{SVM}} = 2.79$). On the other hand, it cannot be neglected that the CPU-time of the test phase of the bare procedure is approximately fifty times the one of the IMSA-SVM because of the need to obtain a detailed map in the whole investigation area $D_1^{(1)}$ instead of in a limited ARoI, $D_1^{(S_{\text{opt}})}$, only. As a matter of fact, the number of test points used by the IMSA approach turns out to be widely reduced.

For completeness, the results from other standard nonlinear classification methods, such as the multilayer perceptron (MLP) and the radial basis functions (RBF) neural network, have been analyzed, as well. More specifically, the DOA probability maps obtained with the MLP-based and RBFNN-based classifiers are reported in Figs. 4(b) and 4(c), respectively. Whatever the method, the achieved estimate does not appear to be adequate and certainly not comparable neither with that of the IMSA-SVM [Fig. 4(b)–(c) versus Fig. 3(b)] nor with that of the bare SVM [Fig. 4(b)–(c) versus Fig. 4(a)] as also

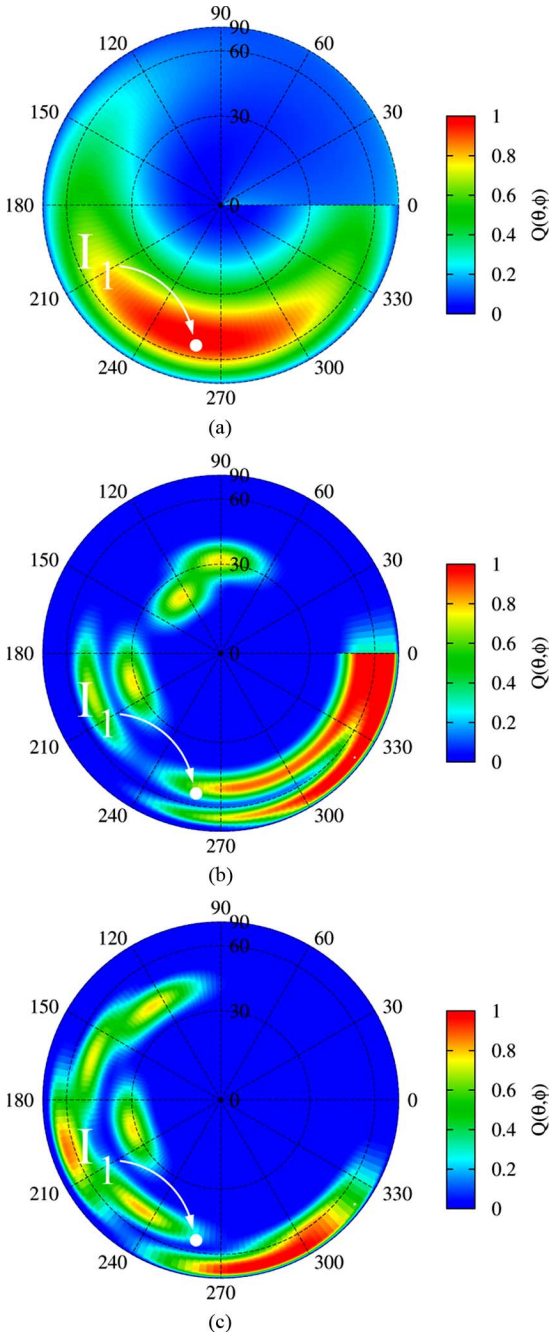


Fig. 4. *Single signal scenario*, $I = 1$—Probability maps obtained with different classification approaches: (a) single-step SVM, (b) MLP neural network, and (c) RBF neural network [$\Delta\theta = 1.25°$ and $\Delta\phi = 5°$].

confirmed by the values of the location index: $\varsigma\rfloor_{RBF} = 10.21$ and $\varsigma\rfloor_{\text{MLP}} = 25.91$.

The last analysis is concerned with the comparison between the IMSA-SVM and those state-of-the-art methods for DOA estimation aimed at determining the angular incidence of the signals, namely MUSIC, ESPRIT (i.e., two one-dimensional ESPRITs independently-applied to the arrays followed by an alignment procedure to associate the estimated azimuth and elevation angle), $2D$-unitary ESPRIT [7], and a support vector regression-based (SVR) approach. Towards this end, the azimuthal direction of the actual signal has been fixed to $\phi = 260°$, while

TABLE II
*SINGLE* SIGNAL SCENARIO, $I = 1$—*COMPARATIVE* ASSESSMENT. VALUES OF THE LOCATION INDEX $\varsigma$ WHEN APPLYING IMSA-DOA, SVR, MUSIC, AND ESPRIT

| | *DOA Method* | | | | | |
|---|---|---|---|---|---|---|
| $\theta_1$ | *ESPRIT* | *2D ESPRIT* | *MUSIC* | *SVR* | $IMSA-SVM^{(unif)}$ | $IMSA-SVM$ |
| $20^o$ | 0.16 | 0.08 | 0.34 | 1.21 | 0.75 | 0.52 |
| $40^o$ | 0.51 | 0.22 | 0.59 | 1.38 | 1.17 | 0.83 |
| $60^o$ | 0.51 | 0.27 | 0.68 | 1.64 | 1.52 | 2.22 |
| $80^o$ | 0.68 | 0.36 | 0.74 | 1.56 | 1.64 | 4.93 |

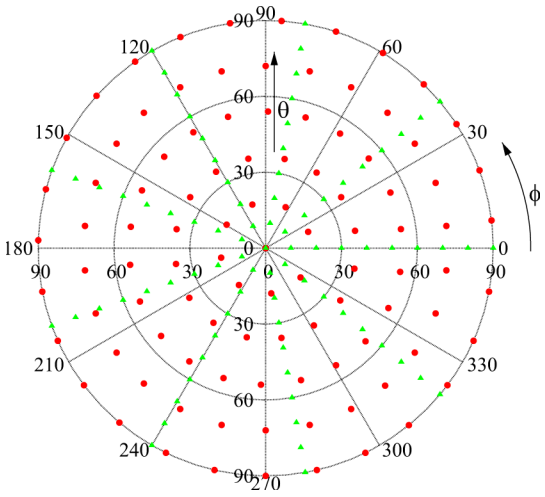


Fig. 5. *Single signal scenario*, $I = 1$—Uniform (points) and nonuniform (triangles) angular training sets.

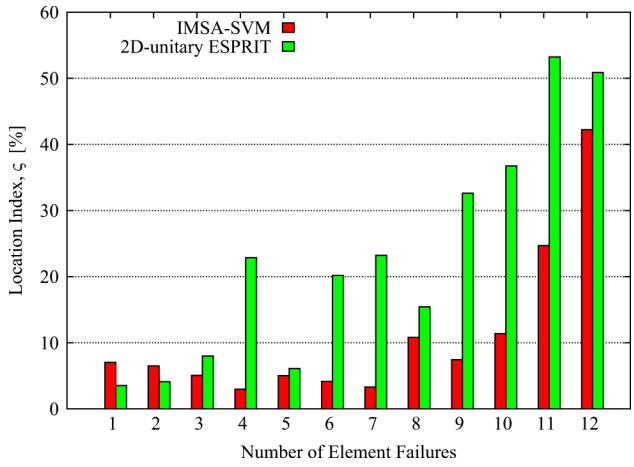


Fig. 6. *Single signal scenario*, $I = 1$—Behavior of the location index versus the number of failed array elements.

the elevation angle has been varied in the range $\theta \in [20° \div 80°]$. Moreover, the SVR algorithm has been previously trained with a dataset composed by $T = T_1 = 100$ examples concerned with only one signal ($I = 1$). The methods are then compared by means of the resulting signal location error, $\varsigma$.

Because of the planar array of isotropic elements and as expected [25], the performances of the DOA techniques in $\theta$ elevation-estimation turn out to better at high elevations ($\theta \to 0°$) [Table II], while the $\phi$ azimuth-estimation is greatest at low elevations ($\theta \to 90°$). Moreover, the values of the estimation indexes point out that the IMSA-SVM (last column—Table II) is able to obtain similar results, in terms of angular resolution, than those provided by the SVR and of the same order in magnitude of MUSIC and ESPRITs except for wider angles ($\theta \geq 60°$), even though these latter need more CPU-time (i.e., an optimized IMSA-SVM implementation just needs few milliseconds on a PC equipped with a 3.0 GHz processor and 2 GHz of RAM). As regards to the growing of the location index around 60°, its mainly depends on the training set. As a matter of fact, it can be avoided by modifying the off-line training phase. For instance, the choice of a uniform angular distribution of the training samples (Fig. 5), instead of a nonuniform arrangement, allows one to obtain a behavior of $\varsigma$ almost invariant to $\theta$ for medium-high elevations.

In order to point out the generalization capabilities of the proposed approach as well as its robustness to the model tolerances [14], [26], the effect of the array failure has been evaluated and the arising results compared to those with *2D-unitary ESPRIT* which demonstrated several advantages over MUSIC and the standard ESPRIT implementation. Towards this end, an increasing number of array elements has been switched off. Moreover, the *a-priori* information on the failure of some array elements has not been exploited through the definition of an ad-hoc training set, but the same nonuniform set of input-output examples concerned with the unperturbed array structure has been used. The results of the comparative assessment when ($\theta_1 = 53°$, $\phi_1 = 260°$) are reported in Fig. 6.

### B. Complex Scenarios—Performance Analysis

The following experiments are aimed at assessing the effectiveness of the IMSA-SVM in detecting the DOAs of multiple signals.

Dealing with the detection of two different incidence points, the first example is concerned with test signals coming from ($\theta_1 = 12°$, $\phi_1 = 165°$) and ($\theta_2 = 82°$, $\phi_2 = 165°$), respectively. The probability maps estimated by the IMSA-SVM at different steps are shown in Fig. 7 together with those obtained with the single-step SVM classification procedure [Fig. 7(d)], the MLP-based approach [Fig. 7(e)], and the RBF technique [Fig. 7(f)]. As expected and confirming the outcomes from the study of the single-signal detection, the multiscaling process allows one to significantly enhance the performances of the single-step classification approaches as pictorially shown in Fig. 7 and quantitatively confirmed by the indexes in Table III. Moreover, it is worth noting that this conclusion is not limited to a particular configuration of incidence angles, but it holds true whatever the two-signals scenario under test.

In order to assess the stability of the proposed approach, a test set composed by $T_2^{(\text{test})} = 100$ examples has been con-

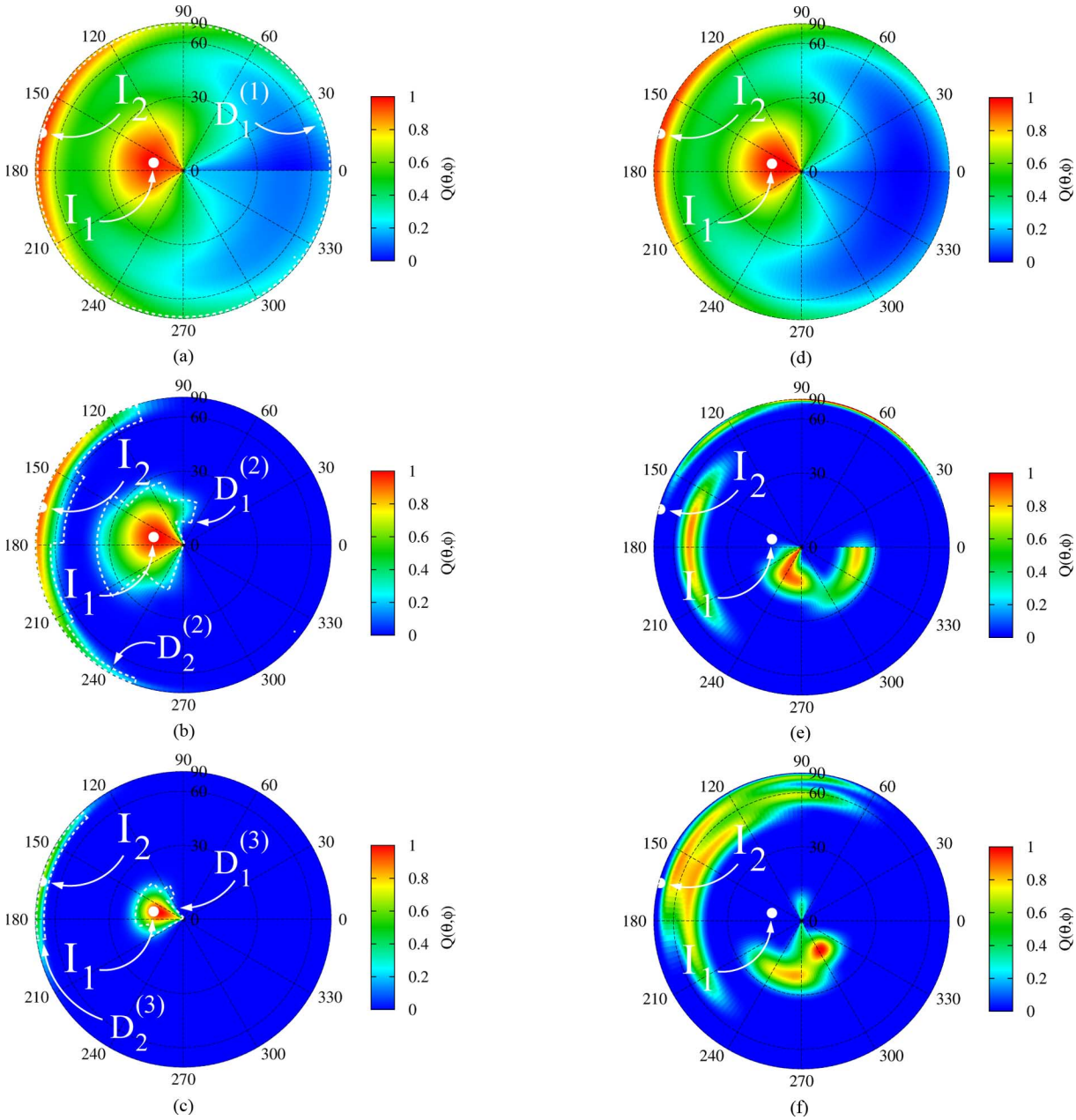


Fig. 7. *Multiple signals scenario*, $I = 2$—Probability maps obtained with different classification approaches: IMSA-SVM [(a) $s = 1$, (b) $s = 2$, (c) $s = S_{\text{opt}} = 3$].

Fig. 7. (*continued*) *Multiple signals scenario*, $I = 2$—Probability maps obtained with different classification approaches: [(d) single-step SVM, (e) multilayer perceptron (MLP) neural network, and (f) radial basis function (RBF) neural network [$\Delta\theta = \Delta\theta_{(2)}^{(3)} = 2.5°$ and $\Delta\phi = \Delta\phi_{(2)}^{(3)} = 10°$].

sidered. The results obtained with the IMSA-SVM are summarized in Table I (second block). As expected, the mean values of the averaged performance indexes ($\hat{\varsigma}_I \triangleq \sum_{i=1}^{I} \varsigma^{(i)}$ and $\hat{\psi}_I \triangleq \sum_{i=1}^{I} \psi^{(i)}$) turn out to be very close to those of the previous test example [i.e., $avg\left(\hat{\varsigma}_2\right) = 4.51$, $avg\left(\hat{\psi}_2\right) = 0.28$ versus $\varsigma_1^{(S_{\text{opt}})} = 4.55$, $\psi_1^{(S_{\text{opt}})} = 0.23$ and $\varsigma_2^{(S_{\text{opt}})} = 3.90$, $\psi_2^{(S_{\text{opt}})} = 0.25$].

The second numerical experiment, concerned with multiple incidences, considers three-signals configurations. As regards to the results for a test set of $T_3^{(\text{test})} = 50$ three-signals examples, the values in the third block of Table I indicate that the resolution accuracy of the proposed approach does not significantly reduce with respect to the single-signal or two-signals scenarios [$avg\left(\hat{\varsigma}_3\right) = 5.55$, $avg\left(\hat{\psi}_3\right) = 0.15$ versus $avg\left(\hat{\varsigma}_2\right) = 4.51$, $avg\left(\hat{\psi}_2\right) = 0.28$ and $\hat{\varsigma}_1 = 2.81$, $\hat{\psi}_1 = 0.25$]. As an illustrative example, let us consider the case of a set of signals impinging on the array from ($\theta_1 = 8°$, $\phi_1 = 85°$), ($\theta_2 = 68°$, $\phi_2 = 95°$), ($\theta_3 = 55°$, $\phi_3 = 290°$). Starting from the coarse map determined, three different ARoIs are successively identified [Fig. 8(a)] and better resolved thus iteratively improving the DOA resolution accuracy as pointed out by the indexes in Table IV where the values estimated by the other classification approaches are reported [Fig. 8(b)], as well. By comparing the distribution at the $S_{\text{opt}}$th step of the IMSA and the one from the bare SVM, it is evident the improvement guaran-

TABLE III
*MULTIPLE* SIGNALS SCENARIO, $I = 2$. PERFORMANCE INDEXES WHEN APPLYING IMSA-DOA, SINGLE-STEP SVM, MLP NEURAL NETWORK, AND RBF NEURAL NETWORK

| *Method* | *DOA Indexes* | | | |
|---|---|---|---|---|
| | $\varsigma_1$ | $\psi_1$ | $\varsigma_2$ | $\psi_2$ |
| $IMSA-SVM$ | | | | |
| $s=1$ | 8.91 | 2.33 | 10.27 | 3.08 |
| $s=2$ | 5.90 | 0.54 | 8.46 | 0.82 |
| $s=S_{opt}=3$ | 4.55 | 0.23 | 3.90 | 0.25 |
| *Bare SVM* | 6.04 | 0.67 | 16.78 | 3.78 |
| *MLP* | 17.54 | 0.27 | 30.53 | 2.21 |
| *RBF* | 17.19 | 0.28 | 27.77 | 0.99 |

TABLE IV
*MULTIPLE* SIGNALS SCENARIO, $I = 3$ (*CONFIGURATION* $1/1/1$). PERFORMANCE INDEXES WHEN APPLYING IMSA-DOA, SINGLE-STEP SVM, MLP NEURAL NETWORK, and RBF NEURAL NETWORK

| | *DOA Indexes* | | | | | |
|---|---|---|---|---|---|---|
| *Method* | $\varsigma_1$ | $\psi_1$ | $\varsigma_2$ | $\psi_2$ | $\varsigma_3$ | $\psi_3$ |
| $IMSA-SVM$ | | | | | | |
| $s=1$ | 5.50 | 0.2 | 5.59 | 1.43 | 4.61 | 1.56 |
| $s=2$ | 4.15 | 0.06 | 5.42 | 0.74 | 4.43 | 0.55 |
| $s=S_{opt}=3$ | 4.24 | 0.009 | 5.19 | 0.33 | 3.10 | 0.14 |
| *Bare SVM* | 10.11 | 0.35 | 4.34 | 1.44 | 16.52 | 1.55 |
| *MLP* | 2.45 | 0.6 | 21.77 | 1.09 | 22.82 | 2.36 |
| *RBF* | 28.31 | 1.35 | 37.34 | 0.49 | 29.57 | 0.67 |

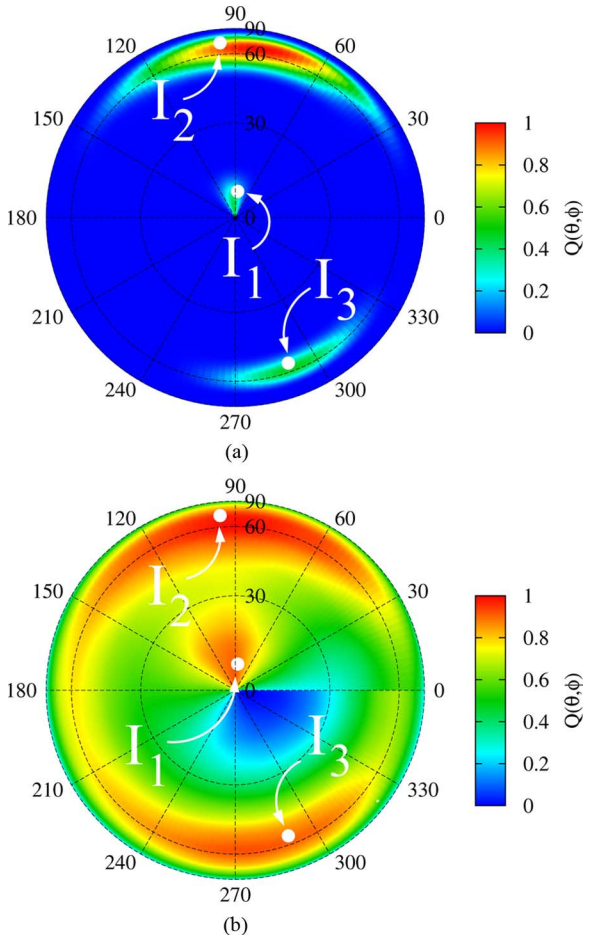


Fig. 8. *Multiple signals scenario*, $I = 3$ (*Configuration* $1/1/1$)—Probability maps obtained with different classification approaches: (a) IMSA-SVM [$s = S_{\text{opt}} = 3$] and (b) single-step SVM [$\Delta\theta = \Delta\theta^{(3)}_{(2)}$ and $\Delta\phi = \Delta\phi^{(3)}_{(2)}$].

teed by the multiscaling process both in resolving and properly locating a number of ARoIs equal to the number of signals ($I$).

In the third experiment, $I = 4$ ($I = I_{\max}$) signals impinge on the planar array. Fig. 9 shows the results provided by the IMSA-SVM and in correspondence with a set of representative examples. More in detail, the first example (*Configuration* $1/1/1/1$) refers to a configuration where four separated signals can be recognized [$(\theta_1 = 35°, \phi_1 = 35°)$, $(\theta_2 = 20°, \phi_2 = 115°)$, $(\theta_3 = 70°, \phi_3 = 135°)$, $(\theta_4 = 80°, \phi_4 = 260°)$ — Fig. 9(a) and (c) ]. The second example [Fig. 9(d)] deals with a two-clusters setup [*Configuration* $2/2$ – $(\theta_1 = 15°, \phi_1 = 75°)$, $(\theta_2 = 25°, \phi_2 = 120°)$, $(\theta_3 = 75°, \phi_3 = 270°)$, $(\theta_4 = 65°, \phi_4 = 300°)$], while a single signal and a cluster of three-signals are present in the last example [*Configuration* $1/3$ – $(\theta_1 = 15°, \phi_1 = 105°)$, $(\theta_2 = 80°, \phi_2 = 275°)$, $(\theta_3 = 85°, \phi_3 = 300°)$, $(\theta_4 = 75°, \phi_4 = 315°)$]. Whatever the example, the multiscaling process is able to identify with an ever increasing resolution from $s = 1$ [Fig. 9(a)] up to $s = S_{\text{opt}} = 3$ [Fig. 9(c)] the ARoIs to which the incidence directions of the actual signals belong as pointed out by the numerical indexes $\psi^{(i)}$, $i = 1, \ldots, I$ in Table V. On the other hand, it should be noticed that the DOA estimation process tends to cluster multiple regions-of-incidence in a single ARoI when the angular separations among the signals reduce. Such an event takes place also in correspondence with the "*Configuration* $2/2$" [Fig. 9(d) and Table VI] where two ARoIs are identified. It is even more evident in Fig. 9(e) (Table VII) where the angular incidences of three signals are detected in only one ARoI. The "clustering" effect is quantitatively pointed out by the behavior of the averaged localization index (Table I—fourth block) when dealing with the complete test set ($T_4^{(\text{test})} = 50$) to which previous examples belong. As a matter of fact, there is a significant increase of the $avg\,(\hat{\varsigma})$ compared to the values of the same quantity when $I = 1, 2, 3$ [$avg\,(\hat{\varsigma}_4) = 17.29$ versus $avg\,(\hat{\varsigma}_1) = 2.81$, $avg\,(\hat{\varsigma}_2) = 4.51$, $avg\,(\hat{\varsigma}_3) = 5.55$], even though the value of $avg\left(\hat{\psi}\right)$ remains close to those of other multiple-signals configurations since the estimated ARoIs still carefully identify the actual incidence areas.

The fourth and fifth experiments deal with more critical test scenarios since the examples under test are concerned with a number of signals different from that in the training set (i.e., $I \neq 1, 2, 3, 4$). More specifically, let us consider the *Clustered Distribution* of $I = 18$ signals with incidence directions indicated by the white points in Fig. 10. It is worth noticing that such a configuration turns out to be not admissible (i.e., $I = 18$ estimates cannot be obtained) for signal subspace-based array processing techniques as *2D-unitary ESPRIT* when the planar

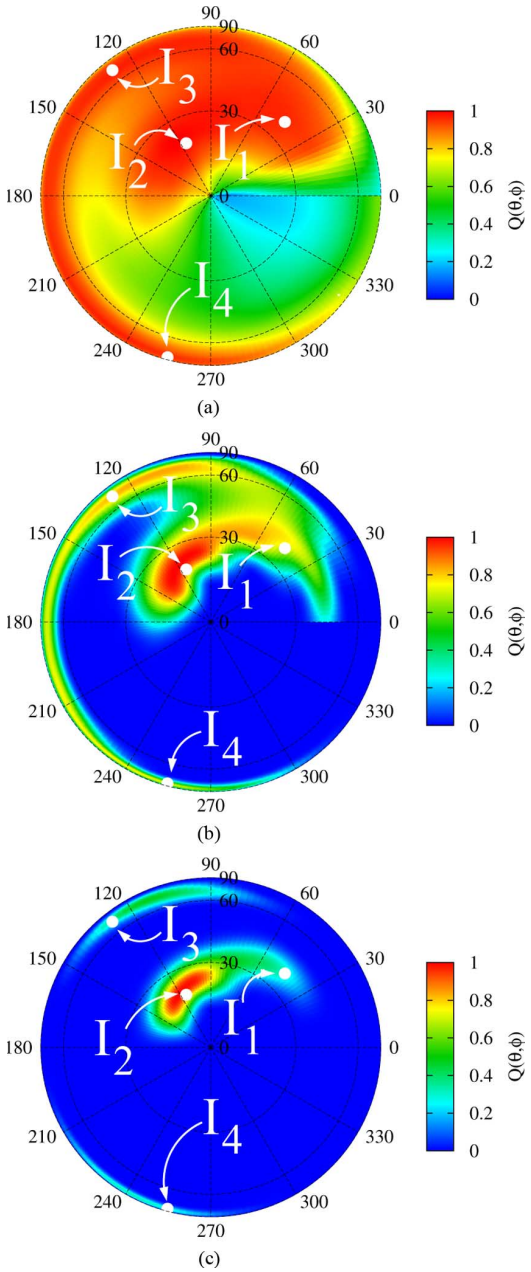


Fig. 9. *Multiple signals scenario* $I = 4$—Probability maps obtained with the IMSA-SVM. *Configuration* $1/1/1/1$: step (a) $s = 1$, (b) $s = 2$, and (c) $s = S_{\text{opt}} = 3$.

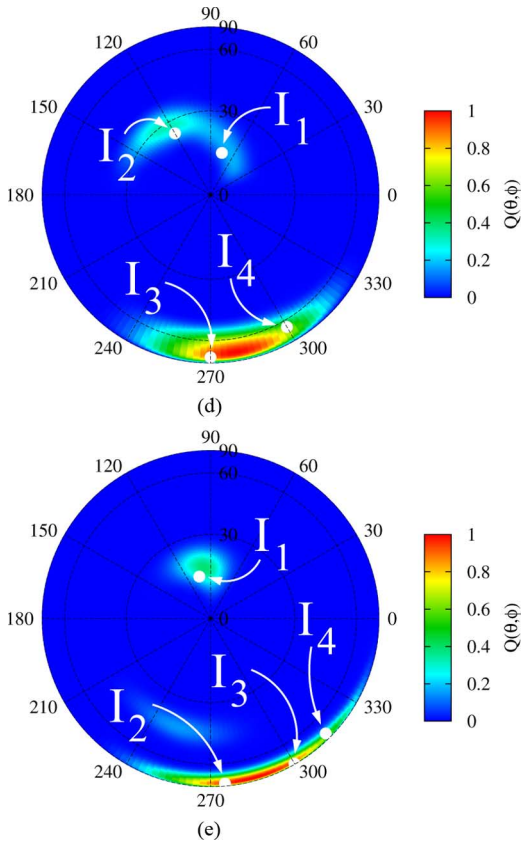


Fig. 9. (*continued*) *Multiple signals scenario* $I = 4$—Probabilitymaps obtained with the IMSA-SVM. *Configuration* $1/1/1/1$:*Configuration* $2/2$: step $s = S_{\text{opt}} = 3$ (d); *Configuration* $1/3$ $s = S_{\text{opt}} = 3$ (e).

TABLE V
*MULTIPLE* SIGNALS SCENARIO, $I = 4$ (*CONFIGURATION* $1/1/1/1$). PERFORMANCE INDEXES WHEN APPLYING IMSA-DOA, SINGLE-STEP SVM, MLP NEURAL NETWORK, AND RBF NEURAL NETWORK

| *Method* | *DOA Indexes* | | | | | | | |
|---|---|---|---|---|---|---|---|---|
| | $\varsigma_1$ | $\psi_1$ | $\varsigma_2$ | $\psi_2$ | $\varsigma_3$ | $\psi_3$ | $\varsigma_4$ | $\psi_4$ |
| $IMSA-SVM$ | | | | | | | | |
| $s=1$ | 6.84 | 0.40 | 24.37 | 0.40 | 23.31 | 1.48 | 25.47 | 1.56 |
| $s=2$ | 5.85 | 0.31 | 28.01 | 0.31 | 16.96 | 0.91 | 8.08 | 0.68 |
| $s=S_{opt}=3$ | 3.44 | 0.16 | 29.33 | 0.16 | 12.31 | 0.21 | 7.42 | 0.24 |
| *Bare SVM* | 8.37 | 2.89 | 24.71 | 2.89 | 26.52 | 2.89 | 25.68 | 2.89 |
| *MLP* | 38.98 | 0.52 | 8.91 | 0.52 | 35.34 | 1.82 | 17.46 | 1.69 |
| *RBF* | 15.19 | 0.32 | 18.69 | 0.32 | 40.65 | 1.81 | 22.01 | 0.91 |

array structure at hand is used. As a matter of fact, the maximum number of sources *2D-unitary ESPRIT* can handle is equal to [7]

$$I_{\max}^{\text{2D ESPRIT}} = \min\{U \times (V-1)\,;\, V \times (U-1)\} \qquad (16)$$

being $M = U \times V$. On the other hand, it should be considered that an high dimensional array processing is enabled widening the size of the planar array (i.e., the number of array sensors) at the expense of the computational complexity that, unlike SVM-based methods, exponentially grows.

Fig. 10 compares the "convergence" ($s = S_{\text{opt}} = 3$) map provided by the IMSA-SVM and the ones from other single-step classifiers. As it can be observed, the multiscaling process is still able to carefully estimate the ARoI to which the actual signals belong with a degree of accuracy higher than that from the other techniques both in terms of localization and area extension (Table VIII). Similar conclusions hold true when dealing with the detection of the signals distribution displayed in Fig. 11, although the detection of the single signal on the bottom of the region of analysis appears to be more critical probably because of the absence of similar spatial configurations in the training set.

Finally, the last experiment is concerned with a scenario where there are not signals that impinge on the array and the noise level has been varied from the reference value used for

TABLE VI
*MULTIPLE* SIGNALS SCENARIO, $I = 4$ (*CONFIGURATION* $2/2$). PERFORMANCE INDEXES WHEN APPLYING IMSA-DOA, SINGLE-STEP SVM, MLP NEURAL NETWORK, AND RBF NEURAL NETWORK

| *Method* | *DOA Indexes* | | | | | | | |
|---|---|---|---|---|---|---|---|---|
| | $\varsigma_1$ | $\psi_1$ | $\varsigma_2$ | $\psi_2$ | $\varsigma_3$ | $\psi_3$ | $\varsigma_4$ | $\psi_4$ |
| $IMSA-SVM$ | | | | | | | | |
| $s=1$ | 15.50 | 0.89 | 11.51 | 0.89 | 45.50 | 2.98 | 57.71 | 2.98 |
| $s=2$ | 12.78 | 0.39 | 10.65 | 0.39 | 10.80 | 0.72 | 24.12 | 0.72 |
| $s=S_{opt}=3$ | 12.91 | 0.16 | 10.55 | 0.16 | 4.71 | 0.26 | 17.01 | 0.26 |
| *Bare SVM* | 15.46 | 0.91 | 11.64 | 0.91 | 46.53 | 3.17 | 58.66 | 3.17 |
| *MLP* | 9.35 | 0.29 | 8.66 | 0.29 | 13.75 | 1.75 | 27.43 | 1.75 |
| *RBF* | 8.06 | 0.26 | 8.77 | 0.26 | 14.84 | 0.57 | 9.50 | 0.57 |

TABLE VII
*MULTIPLE* SIGNALS SCENARIO, $I = 4$ (*CONFIGURATION* $1/3$). PERFORMANCE INDEXES WHEN APPLYING IMSA-DOA, SINGLE-STEP SVM, MLP NEURAL NETWORK, AND RBF NEURAL NETWORK.

| *Method* | *DOA Indexes* | | | | | | | |
|---|---|---|---|---|---|---|---|---|
| | $\varsigma_1$ | $\psi_1$ | $\varsigma_2$ | $\psi_2$ | $\varsigma_3$ | $\psi_3$ | $\varsigma_4$ | $\psi_4$ |
| $IMSA-SVM$ | | | | | | | | |
| $s=1$ | 16.98 | 0.88 | 39.13 | 2.81 | 54.57 | 2.81 | 64.78 | 2.81 |
| $s=2$ | 16.51 | 0.62 | 6.04 | 1.70 | 22.43 | 1.70 | 35.70 | 1.70 |
| $s=S_{opt}=3$ | 8.13 | 0.59 | 6.18 | 1.46 | 11.84 | 1.46 | 28.89 | 1.46 |
| *Bare SVM* | 17.38 | 0.87 | 39.45 | 2.85 | 54.87 | 2.85 | 65.72 | 2.85 |
| *MLP* | 11.62 | 0.19 | 27.46 | 1.08 | 11.41 | 1.08 | 8.15 | 1.08 |
| *RBF* | 6.51 | 0.10 | 16.85 | 0.10 | 3.01 | 0.10 | 20.63 | 0.10 |

the SVM training [$P_n = 20$ dB (*Test Set*) versus $P_n = 0$ dB (*Training Set*)] thus further complicating the test case. As a matter of fact, neither the free-case example is present in the training set nor the same noise level has been "learned." Nonetheless, the SVM-based classifier did not detected the presence of any signal thus defining a uniform distribution of probability [Fig. 12(a)]. Otherwise, the other methods give color-maps with some "artifacts" [see Fig. 12(b) and (c)] although characterized by very small values of the probability of signal incidence.

### C. Dipole Array Antenna

In the last experiment, a uniform array of $\lambda$ 2-dipoles is taken into account with dipoles oriented along the $x$ axis. Therefore, the effective length [24] of the array element turns out to be

$$\underline{e}_m = \frac{\lambda}{\pi}\left[\frac{\cos\left(\frac{\pi}{2}\sin\theta\cos\phi\right)}{1-\sin^2\theta\cos^2\phi}\right]\left[(\cos\theta\cos\phi)\,\underline{\theta} - (\sin\phi)\,\underline{\phi}\right]. \tag{17}$$

Moreover, the inter-element distance has been chosen equal to $d_x = 0.65\lambda$ and $d_y = 0.5\lambda$ [27]. Then, a subset of the experiments of the previous sections, but with the dipole array, has been dealt with to evaluate the applicability of the IMSA-SVM approach to nonideal electromagnetic scenarios, as well.

In the first example ($I = 1$), the multiscaling procedure stops after $S_{\text{opt}} = 4$ iterations and the final result is shown in Fig. 13. Likewise the case with point-like sources, the estimations of both the location and the incidence area improve at each iteration starting from $\varsigma^{(1)} = 43.19$ and $\psi^{(1)} = 2.48$ down

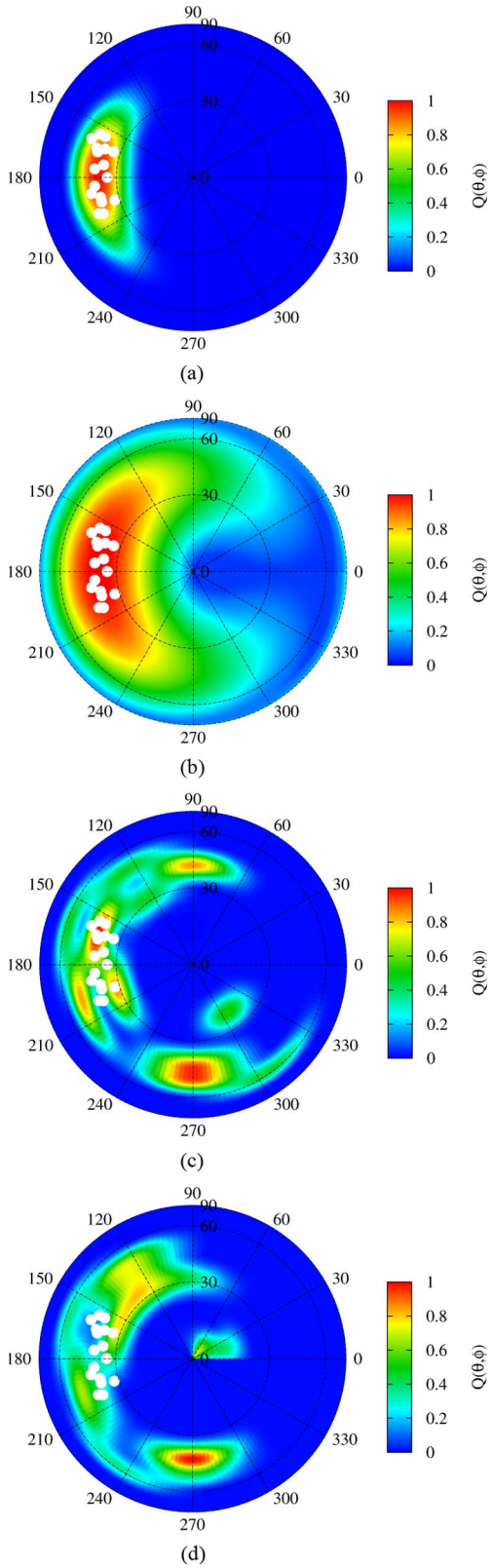


Fig. 10. *Multiple signals scenario* ($I = 18$—*Clustered Distribution*) —Probability maps obtained with different classification approaches: (a) IMSA-SVM ($s = S_{\text{opt}} = 3$), (b) single-step SVM, (c) MLP neural network, and (d) RBF neural network [$\Delta\theta = \Delta\theta^{(3)}_{(2)}$ and $\Delta\phi = \Delta\phi^{(3)}_{(2)}$].

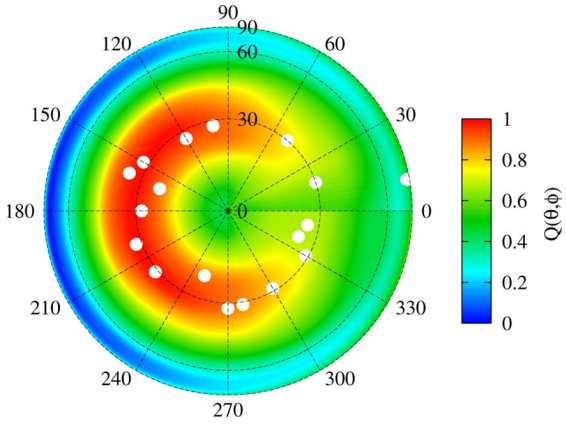


Fig. 11. *Multiple signals scenario* ($I = 18$ — *Sparse Distribution*) — Probability maps determined by the IMSA-SVM at the convergence ($s = S_{\text{opt}} = 2 - \Delta\theta_{(1)}^{(2)} = 5°$ and $\Delta\phi_{(1)}^{(2)} = 20°$).

TABLE VIII
*MULTIPLE* SIGNALS SCENARIO, $I = 18$ (*CLUSTERED* DISTRIBUTION). PERFORMANCE INDEXES WHEN APPLYING IMSA-DOA, SINGLE-STEP SVM, MLP NEURAL NETWORK, AND RBF NEURAL NETWORK.

| *Method* | *DOA Indexes* | |
|---|---|---|
| | $\hat{\varsigma}$ | $\hat{\psi}$ |
| $IMSA-SVM$ | 1.20 | 0.21 |
| *Bare SVM* | 2.82 | 1.94 |
| $MLP$ | 13.78 | 1.66 |
| $RBF$ | 13.62 | 1.21 |

to $\varsigma^{(S_{\text{opt}})} = 2.96$ and $\psi^{(S_{\text{opt}})} = 0.06$, where $\varsigma^{(2)} = 12.65$, $\varsigma^{(3)} = 5.41$ and $\psi^{(2)} = 0.75$, $\psi^{(3)} = 0.21$. In this case, the performance are comparable to that in Section III-A. Different conclusions arise when processing the data of the two-signal scenario [Fig. 14(a)]. In such a case, only the $I_1$ (i.e., the signal with the lowest elevation $\theta$) is detected [Fig. 14(a)]. Such an event does not depend on the DOA detection method, but from the antenna array at hand. As a matter of fact, the radiation pattern of the array element is omnidirectional in the $z-y$ plane (i.e., $\phi = 90°$ and $\phi = 270°$) with a $\theta_{3\text{ dB}}$ angle of almost 80° degrees [24]. Therefore, the gain of the dipole is lower along the direction with higher $\theta$s, being $\phi_1 = \phi_2 = 165°$. Otherwise, when the actual configuration is described by a set of signals coming from the directions $(\theta_1 = 30°,\ \phi_1 = 60°)$ and $(\theta_2 = 30°,\ \phi_2 = 300°)$, the IMSA-SVM method still gives accurate estimates [Fig. 14(b)] although with non-ideal isotropic receiving sensors.

## IV. CONCLUSION

In this paper, a multiresolution approach for the DOA estimation of multiple signals based on a support vector classifier has been presented. The procedure is aimed at defining a probability map of the incidence of an electromagnetic signal on a planar array of sensors. Starting from a coarse map, a synthetic zoom is iteratively performed in the angular sector where the incidence of a signal has been detected with higher probability at the previous step of the multiscaling procedure.

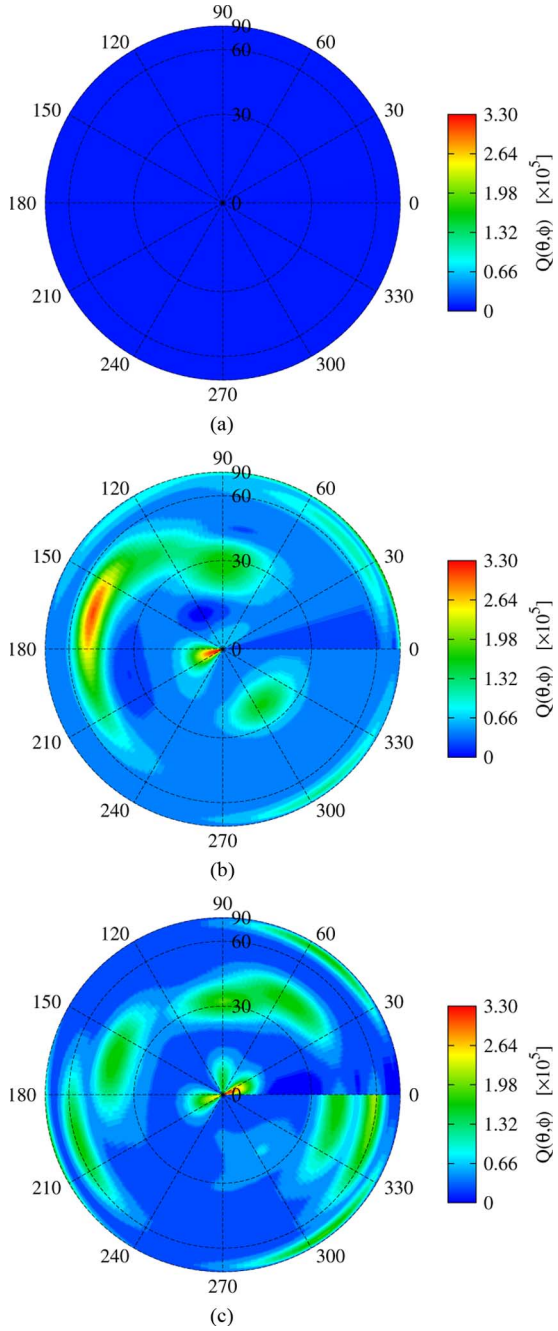


Fig. 12. *No-signals scenario* [$I = 0$; $P_n = 20$ dB (*Test Set*) — $P_n = 0$ dB (*Training Set*)] — Probability maps obtained with different classification approaches: (a) IMSA-SVM ($s = S_{\text{opt}} = 1$), (b) MLP neural network, and (c) RBF neural network.

The effectiveness of the proposed approach has been assessed dealing with different scenarios and working conditions. Moreover, a comparative analysis has been carried out by considering state-of-the-art DOA methods. The obtained results have shown that:

- the use of a classifier based on SVM allows one to estimate the DOA probability map in real time;
- thanks to the SVM generalization capability, the IMSA-SVM behaves properly when dealing with complex electromagnetic scenarios non-necessarily belonging to the set of training examples;

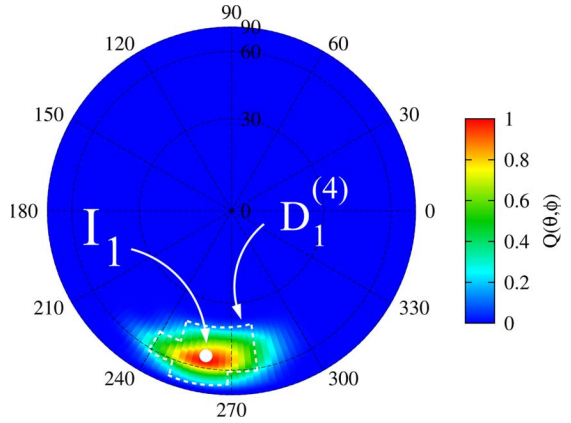


Fig. 13. *Dipole Array, $I = 1$*—Probability map determined by the IMSA-DOA [$s = S_{\text{opt}} = 4$].

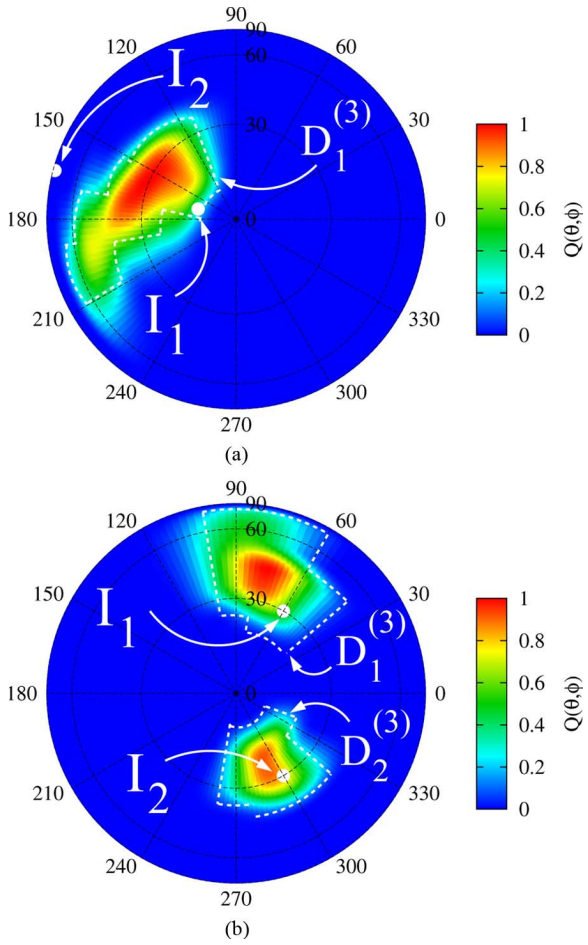


Fig. 14. *Dipole Array, $I = 2$*—Probability map determined by the IMSA-DOA when (a) $I_1 = (\theta_1 = 12°, \phi_1 = 165°)$, $I_2 = (\theta_2 = 82°, \phi_2 = 165°)$ [$s = S_{\text{opt}} = 3$] and (b) $I_1 = (\theta_1 = 30°, \phi_1 = 60°)$, $I_2 = (\theta_2 = 30°, \phi_2 = 300°)$ [$s = S_{\text{opt}} = 3$].

- the SVM-based approach is able to estimate the DOAs of a number of sources greater than the maximum allowed by conventional eigenvalue decomposition methods for a fixed planar array geometry;
- unlike $2-D$ subspace-based algorithms, the computational complexity does not increase with the size of the rectangular array;
- the proposed LBE technique adapts to element failure or other source of errors coming from the tolerances in the array structure that cause non-negligible performance degradation in conventional estimation techniques which require highly calibrated antennas with identical radiation properties;
- the *a-priori* knowledge (deterministic or statistical) on the array configuration and radiation pattern characteristics can be easily and usefully exploited by defining suitable IMSA-SVM training sets;
- the multiscaling procedure (IMSA) provides good results dealing with both single-signal and multiple-signals configurations with an angular resolution comparable to that of other state-of-the-art DOA algorithms;
- system complexity, classifier architecture, and computational costs significantly reduce with respect to the "bare" classification.

## ACKNOWLEDGMENT

The authors wish to thank the reviewers for many valuable suggestions and comments that helped improve this paper. In addition, discussions with Dr. L. Lizzi and Dr. Oliveri are much appreciated.

## REFERENCES

[1] M. Chryssomallis, "Smart antennas," *IEEE Antennas Propag. Mag.*, vol. 42, no. 3, pp. 129–136, Jun. 2000.
[2] E. L. Hines, M. S. Leeson, M. M. Ramon, M. Pardo, E. Llobet, D. D. Iliescu, and J. Yang, *Intelligent Systems: Techniques and Applications*. Maastricht, Germany: Shaker, 2008.
[3] S. P. Applebaum, "Adaptive arrays," *IEEE Trans. Antennas Propag.*, vol. 24, no. 5, pp. 585–598, May 1976.
[4] D. S. Weile and E. Michielssen, "The control of adaptive antenna arrays with genetic algorithms using dominances and diploidy," *IEEE Trans. Antennas Propag.*, vol. 49, no. 10, pp. 1424–1433, Oct. 2003.
[5] R. Roy and T. Kailath, "ESPRIT-Estimation of signal parameters via rotational invariance techniques," *IEEE Trans. Acoust., Speech, Signal Process.*, vol. 37, no. 7, pp. 984–995, Jul. 1989.
[6] F. Gao and B. Gershman, "A generalized ESPRIT approach to direction-of-arrival estimator," *IEEE Signal Process. Lett.*, vol. 12, no. 3, pp. 254–257, Mar. 2005.
[7] M. D. Zoltowski, M. Haardt, and C. P. Mathews, "Closed-form 2-D angle estimation with rectangular arrays in element space or beamspace via unitary ESPRIT," *IEEE Trans. Signal Process.*, vol. 44, no. 2, pp. 316–328, Feb. 1996.
[8] R. O. Schmidt, "Multiple emitter location and signal parameter estimation," *IEEE Trans. Antennas Propag.*, vol. 34, no. 3, pp. 276–280, Mar. 1986.
[9] A. Swindlehurst and T. Kailath, "A performance analysis of sub space-based methods in the presence of model errors. I. The MUSIC algorithm," *IEEE Trans. Signal Process.*, vol. 40, no. 7, pp. 1578–1774, Jul. 1992.
[10] I. Ziskind and M. Wax, "Maximum likelihood localization of multiple sources by alternating projection," *IEEE Trans. Acoust., Speech, Signal Process.*, vol. 36, no. 10, pp. 1553–1560, Oct. 1988.
[11] P. Stoica and A. B. Gershman, "Maximum-likelihood DOA estimation by data-supported grid search," *IEEE Signal Process. Lett.*, vol. 6, no. 10, pp. 273–275, Oct. 1999.
[12] A. H. El Zooghby, C. G. Christodoulou, and M. Georgiopulos, "Performance of radial-basis function networks for direction of arrival estimation with antenna arrays," *IEEE Trans. Antennas Propag.*, vol. 45, no. 11, pp. 1611–1617, Nov. 1997.
[13] A. H. El Zooghby, C. G. Christodoulou, and M. Georgiopulos, "A neural network-based smart antenna for multiple source tracking," *IEEE Trans. Antennas Propag.*, vol. 48, pp. 768–776, May 2000.

[14] M. Martinez-Ramon and C. G. Christodoulou, *Support Vector Machines for Antenna Array Processing and Electromagnetics Synthesis Lectures on Computational Electromagnetics Lecture # 5*. San Rafael, CA: Morgan & Claypool, 2006.
[15] V. Vapnik, *Statistical Learning Theory*. New York: Wiley, 1998.
[16] E. Bermani, A. Boni, S. Caorsi, M. Donelli, and A. Massa, "A multi-source strategy based on a learning-by-examples technique for buried object detection," in *Progr. Electromagn. Res.*. Philadelphia, PA: PIER, 2004, vol. 48, pp. 185–200.
[17] A. Massa, A. Boni, and M. Donelli, "A classification approach based on SVM for electromagnetic subsurface sensing," *IEEE Trans. Geosci. Remote Sens.*, vol. 43, no. 9, pp. 2084–2093, Sep. 2005.
[18] D. Anguita, A. Boni, and S. Ridella, "A digital architecture for support vector machines: Theory, algorithm and FPGA implementation," *IEEE Trans. Neural Netw.*, vol. 14, no. 5, pp. 993–1009, Sep. 2003.
[19] M. Pastorino and A. Randazzo, "A smart antenna system for direction of arrival estimation based on a support vector regression," *IEEE Trans. Antennas Propag.*, vol. 53, no. 7, pp. 2161–2168, Jul. 2005.
[20] M. Pastorino and A. Randazzo, "The SVM-based smart antenna for estimation of the directions of arrival of electromagnetic waves," *IEEE Trans. Instrum. Meas.*, vol. 55, pp. 1918–1925, Dec. 2006.
[21] A. Randazzo, M. A. Abou-Khousa, M. Pastorino, and R. Zoughi, "Direction of arrival estimation based on support vector regression: Experimental validation and comparison with MUSIC," *IEEE Trans. Antennas Wireless Propag. Lett.*, vol. 6, pp. 379–382, 2007.
[22] S. Caorsi, M. Donelli, D. Franceschini, and A. Massa, "A new methodology based on an iterative multiscaling for microwave imaging," *IEEE Trans. Microw. Theory Tech.*, vol. 51, no. 4, pp. 1162–1173, Apr. 2003.
[23] L. C. Godara, "Applications of antenna arrays to mobile communications—Part I: Performance improvement, feasibility, and system considerations," *Proc. IEEE*, vol. 85, pp. 1031–1060, Jul. 1997.
[24] C. A. Balanis, *Antenna Theory: Analysis and Design*. New York: Wiley, 2005.
[25] A. Manikas, A. Alexiou, and H. R. Karimi, "Comparison of the ultimate direction-finding capabilities of a number of planar array geometries," *Proc. Inst. Elect. Eng. Radar, Sonar Navig.*, vol. 144, no. 6, pp. 321–329, Dec. 1997.
[26] C. G. Christodoulou and M. Georgiopoulos, *Applications of Neural Networks in Electromagnetics*. Boston, MA: Artech House, 2001.
[27] W. Chen, J. Jen, and S. M. Zhang, "Planar dipole arrays with equal element input impedances," *Electron. Lett.*, vol. 31, no. 24, pp. 2061–2062, 1995.

**Massimo Donelli** (M'04) received the Electronic Engineering degree and the Ph.D. degree in space science and engineering from the University of Genoa, Italy, in 1998 and 2003, respectively.

He is with the Department of Information and Communication Technology, University of Trento, Italy. His main interests are electromagnetic inverse scattering, adaptive antennas synthesis, optimization techniques for microwave imaging, wave propagation in superconducting materials and urban environment.

**Federico Viani** was born in Trento, Italy, in 1981. He received the M.S. degree in telecommunications engineering from the University of Trento, Italy, in 2007.

He is a member of the ELEDIA Research Group, University of Trento, and his main interests are in antennas synthesis and design, ultrawideband communications and wireless sensor networks.

**Paolo Rocca** received the B.S. and M.S. degrees in telecommunications engineering both from the University of Trento, Italy, in 2004 and 2005, respectively, and the Ph.D. degree from the International Graduate School in Information and Communication Technologies, University of Trento, in 2008.

He is a member of the ELEDIA Research Group, University of Trento. His main interests are in the framework of array antenna synthesis and design, optimization techniques for electromagnetics, electromagnetic inverse scattering.

**Andrea Massa** (M'03) received the "Laurea" degree in electronic engineering and the Ph.D. degree in electronics and computer science from the University of Genoa, Genoa, Italy, in 1992 and 1996, respectively.

From 1997 to 1999, he was an Assistant Professor of Electromagnetic Fields at the Department of Biophysical and Electronic Engineering, University of Genoa, teaching the university course of Electromagnetic Fields 1. From 2001 to 2004, he was an Associate Professor at the University of Trento, Trento, Italy. Since 2005, he has been a Full Professor of Electromagnetic Fields at the University of Trento, where he currently teaches electromagnetic fields, inverse scattering techniques, antennas and wireless communications, and optimization techniques. At present, he is the Director of the ELEDIALab at the University of Trento and Deputy Dean of the Faculty of Engineering. His research work since 1992 has been principally on electromagnetic direct and inverse scattering, microwave imaging, optimization techniques, wave propagation in presence of nonlinear media, wireless communications and applications of electromagnetic fields to telecommunications, medicine and biology.

Dr. Massa is a member of the PIERS Technical Committee, the European Microwave Association (EuMA), and of the Inter-University Research Center for Interactions Between Electromagnetic Fields and Biological Systems (ICEmB).